Facile fluorescent detection of *o*-nitrophenol by a cucurbit[8]uril-based supramolecular assembly in aqueous media

Jiao He [a], *Xiang-Yun Yu* [a], *Zhi-Chao Yu* [a], *Ming Liu* [a], *Pei-Hui Shan* [a], *Carl Redshaw* [b], *Ying Huang* [a], *Zhu Tao* [a], *Xin Xiao*[*a].

[a] Key Laboratory of Macrocyclic and Supramolecular Chemistry of Guizhou Province, Institute of Applied Chemistry, Guizhou University, Guiyang 550025, China.

[b] Department of Chemistry, University of Hull, Hull HU6 7RX, U.K.

KEYWORDS: cucurbit[n]urils; pyrene; host-guest interaction; fluorescent probe; nitrophenol isomers

ABSTRACT: The efficient and selective detection of isomers is an attractive but challenging area. In this study, a supramolecular fluorescent probe based on cucurbit[8]uril (Q[8]) and a pyrene-based derivative (G) was prepared, which effectively recognized and removed *o*-nitrophenol (*o*-NP) from a mixture of nitrophenol isomers. The newly designed probe G@Q[8] was characterized by NMR spectroscopy, fluorescence emission and UV-Vis spectroscopy, and its host-guest properties in aqueous solution were investigated. The results revealed that the system forms a stable inclusion complex with a stoichiometric ratio of 1:1, which was accompanied by a distinct fluorescence enhancement of G. Moreover, it was employed for the rapid detection of nitrophenol isomers where *o*-NP showed a dramatical quenching efficiency with a detection limit of 1.53×10^{-7}mol L^{-1}. This highly efficient supramolecular fluorescent probe offers a new strategy for the convenient detection and removal of *o*-NP from mixtures in aqueous medium.

1. Introduction

Isomerism is common in organic chemistry, and it is extremely intriguing and challenging to establish a facile distinction protocol for isomers of organic compounds due to their similar structures and properties [1]. The isomers of nitrophenol, including *o*-nitrophenol (*o*-NP), *m*-nitrophenol (*m*-NP) and *p*-nitrophenol (*p*-NP), are widely employed to synthesize pharmaceuticals, pesticides, herbicides and dyes [2-8]. Owing to their high stability and immunity to microbial degradation [9], they are ubiquitous in the ecological environment, which may cause health problems to humans even at low concentrations, such as headache, nausea, cyanosis, and even liver or kidney damages [10-11]. Additionally, they are also extremely harmful to animals and plants [12]. On account of this, the discrimination and selective detection of trace levels of nitrophenol isomers is essential for environmental control and human health issues. However, the structural properties of the isomers of nitrophenol make it difficult to achieve their individual or simultaneous detection [13]. Thus, it remains a great challenge to develop a precise and effective analytical technique for the individual or simultaneous determination of the three isomers of nitrophenol.

To date, various strategies have been proposed for the detection and distinction of the isomers of nitrophenol, including UV–vis spectrophotometry [14], gas chromatography [15-16], magnetic circular dichroism [17-18], high-performance liquid chromatography [19], electrochemical analysis [20-21], capillary electrophoresis [22] and so on. However, these methods are usually time-consuming, and require sophisticated and costly instrumentation, and suffer from complex operations during practical applications. As a consequence, simple, inexpensive, and convenient methods to discriminate between and detect nitrophenol isomers are still in demand. In comparison, the method of using a fluorescent probe to detect organics has attracted growing interest, because it is faster, simpler, cheaper, more sensitive and selective [23-26]. Several fluorescent probes exhibiting satisfying results for the discrimination between organic isomers have been reported [27]. For example, Yuan *et al* constructed a novel AuNC-based fluorescent sensor array for the efficient discrimination of three nitrophenol isomers [28]. Zhang *et al* reported a novel chemical sensor based on a fluorescent metal-organic framework for the selective distinction between and analysis of *o*-xylene and xylene isomers [29]. Zhang and co-workers prepared a novel carbon dot decorated chiral porous organic cage hybrid nanocomposite and used it to fabricate a fluorescent probe for the rapid

differentiation of nitrophenol isomers [30]. Therefore, development of a novel fluorescent probe for distinguishing and detecting nitrophenol isomers has broad prospects.

Cucurbit[*n*]urils (Q[*n*]s, n = 5-8, 10, 13-15), a family of rigid macrocyclic host molecules, are composed of n glycoluril rings connected by 2n methylene bridges. Because of their highly rigid molecular skeleton and great versatility in molecular recognition [31-33], they can form stable host-guest complexes in aqueous solution with a vast number of inorganic and organic guest molecules with highly tunable binding affinities [34-36] including drug guest molecules [37-38] peptide guests [39], and dye guests [40]. They are thus widely used as host molecules to construct supramolecular assemblies. Pyrene is a typical conjugated polycyclic aromatic compound with high quantum efficiency and long fluorescence lifetime [41]. Due to its unique spectral characteristics and chemical stability, it has been widely used in the development and construction of high-emission conjugated molecules for fluorescent probes [42-44]. Hence, in order to combine the advantages of both cucurbit[*n*]urils and pyrene, we designed and synthesized the target molecule 1,6-bis(*N*-hexanoic acid pyridinium-4-yl) pyrene (abbreviated as G), and combined it with Q[8]. This led to the successful construction of the supramolecular fluorescent probe G@Q[8] in aqueous solution with a molar ratio of 1:1 (Scheme 1). Interestingly, we found that the probe not only possesses excellent optical properties, but also can effectively identify *o*-NP among three nitrophenol isomers.

Herein, a new pyrene-based derivative molecule G with good water-solubility and excellent optical performance was synthesized, and was utilized to construct a novel host-guest supramolecular fluorescent probe with Q[8] (G@Q[8]). The probe can form a ternary complex with *o*-NP in the aqueous system to achieve the purpose of detecting and removing *o*-NP. It is worth noting that G@Q[8] exhibits favorable differentiation ability towards *o*-NP among the three isomers. The fluorescent probe G@Q[8] provides a simple and convenient strategy for the preparation of *o*-NP fluorescent probes for future research.

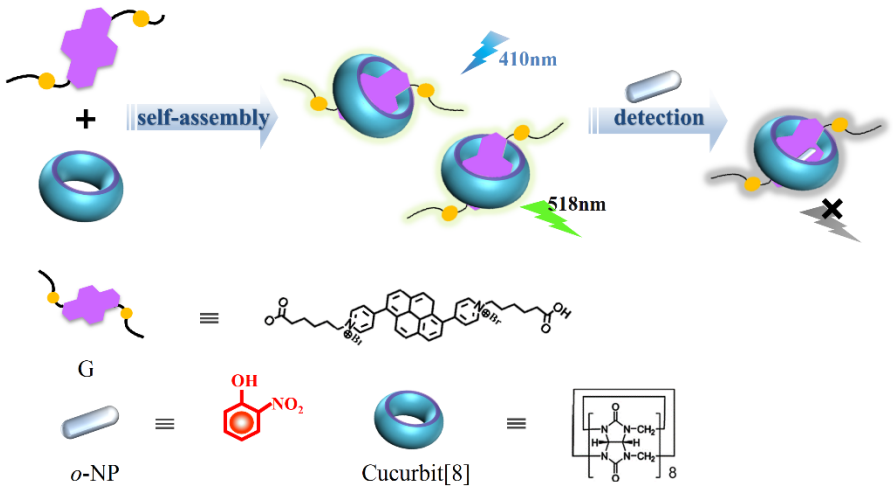

Scheme 1. Schematic diagram of the supramolecular fluorescent probe for the detection of *o*-nitrophenol, and the chemical structures of G and Q[8].

2. Results and discussion

2.1. Molecular design and synthesis

Pyrene is a water-insoluble molecule, so for the purpose of interaction with Q[8] and detection in an aqueous system, we attempted to introduce pyridinium into the pyrene molecule by a Suzuki coupling reaction to prepare 1,6-bis(4′-pyridyl)pyrene (1) [46], and then combining it with 6-bromohexanoic acid in a mixed solvent system of acetonitrile and toluene, and refluxing the reaction to afford the target product G with good water solubility. The synthetic route and ^{1}H NMR spectroscopic characterization is shown in Figures S1-S3 (Supporting Information). Fortunately, we also obtained single crystals suitable for a structure determination. The structure of 2{G•$[ZnCl_4]^{2-}$} was obtained by the addition of Zn(II) chloride to a HCl (6 M) solution containing G. The single crystals of 2{G•$[ZnCl_4]^{2-}$} were found to be in a monoclinic cell and the structure determination was carried out in the space group *I*2/a. The asymmetric unit consists of two G cations and two $[ZnCl_4]^{2-}$ counterions, and the stacking of the structure is shown in Figures 1a-c. In a single crystal, all G molecules exist in a cross-overlapping dimer, and the G molecules are connected to each other by π-π stacking. Different G dimers are further linked together by hydrogen bonds O-H•••O and O-H•••C. There are π…π interactions between the centroids of the

two pyrene rings and between the pyridine ring and the pyrene ring, with short contacts at 3.386 Å and 2.858 Å, respectively (Figure 1d).

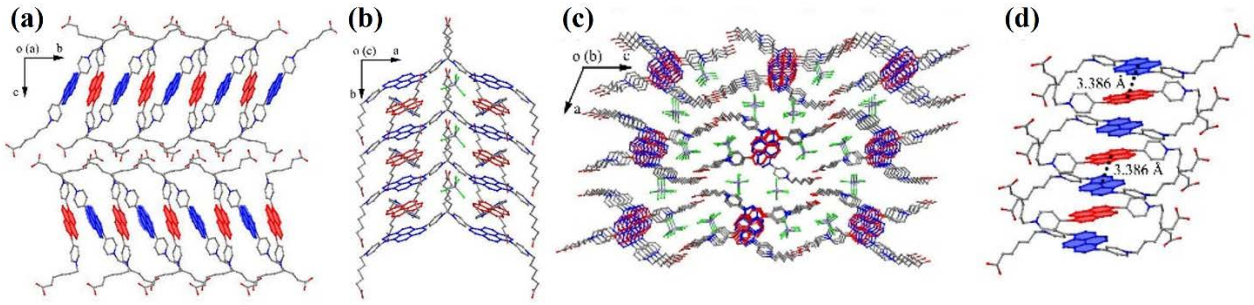

Figure 1. (a, b) Single crystal structure of the G: 2D network stacked structure constructed from G and $[ZnCl_4]^{2-}$ along different directions; (c) 3D structure diagram; (d) Packing diagram shows the strong π…π interactions.

2.2. Host-guest interaction study

The ability of guest G to form a host-guest inclusion complex with Q[8] was firstly monitored by ^{1}H NMR spectroscopic titrations (Figure 2), whereby Q[8] was incrementally added to a 0.5 mM solution of the guest G in D_2O. With the continuous addition of Q[8], the proton chemical shifts of guest G change until the addition of 1.0 equiv. of Q[8]. The proton signals of the alkyl chain of guest G, namely H_g, H_h, H_i and H_j experienced a down-field shift from 2.02, 1.35, 1.58, 2.27 ppm to 2.12, 1.46, 1.64 and 2.33 ppm, respectively. By contrast, the proton signals of the pyrene moiety of the guest G, H_c, H_d and H_e exhibited obvious up-field shifts. It is worth noting that the proton signals of H_a and H_b of the pyridine of guest G all underwent a down-field shift. This indicates that when compared with the free guest G, following the addition of Q[8], the pyrene moiety of G was accommodated within the cavity of the Q[8] and the pyridine moiety was located at the portals of Q[8].

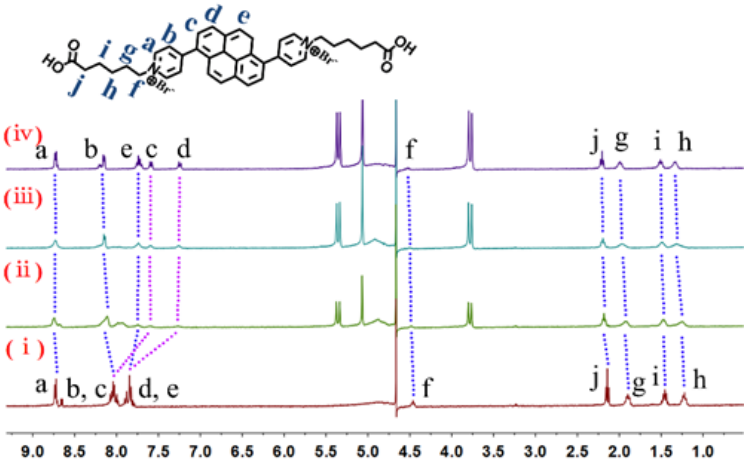

Figure 2. ^{1}H NMR titration spectra (400 MHz, D_2O) of (i) neat G (0.5mM); (ii) G with 0.3 equiv. of Q[8]; (iii) G with 0.7 equiv. of Q[8]; (iv) G with 1.0 equiv. of Q[8].

The interaction between host Q[8] and guest G was further verified by fluorescence emission and UV-Vis spectroscopy. As shown in Figure 3a, the system displays an emission peak at 518 nm in aqueous solution at an excitation wavelength of 410 nm. With the gradual addition of Q[8], the π-π stacking of the pyrene moiety of G is inhibited causing its emission to gradually enhance until it reached a maximum at a Q[8]/G ratio of 1:1, accompanied by a blue shift from 518 nm to 507 nm. A Job's plot further corroborated the stoichiometry of the host-guest inclusion complex (Figure 3c). UV-Vis spectroscopy experiments was also carried out in order to confirm that the molar ratio of the interaction between Q[8] and G is 1:1. As shown in Figure 3d, the maximum absorption wavelengths at 244, 299, 384 and 410 nm all decreased remarkably and generated bathochromic shifts on gradual addition of Q[8], which was attributed to the suppression of rotation and vibration of G when included in the finite cavity of the Q[8] [45]. It was further confirmed by a Job's plot (Figure 3f). In addition, isothermal titration calorimetry (ITC) was used to explore the related thermodynamic parameters of G@Q[8]. As shown in Table S1, the association constant (K_a) between Q[8] and G was $(3.52\pm0.02)\times10^6$ M^{-1}, and the large negative values of ΔH indicate that the interaction between G and Q[8] is mainly driven by favorable enthalpy changes [47-48]. In addition, the value of n is 1.08, which further confirms that the actual ratio of G to Q[8] is 1:1. Based on the above analysis, we mixed G and Q[8] in an aqueous solution with a stoichiometry of 1:1 to fabricate the fluorescent probe G@Q[8].

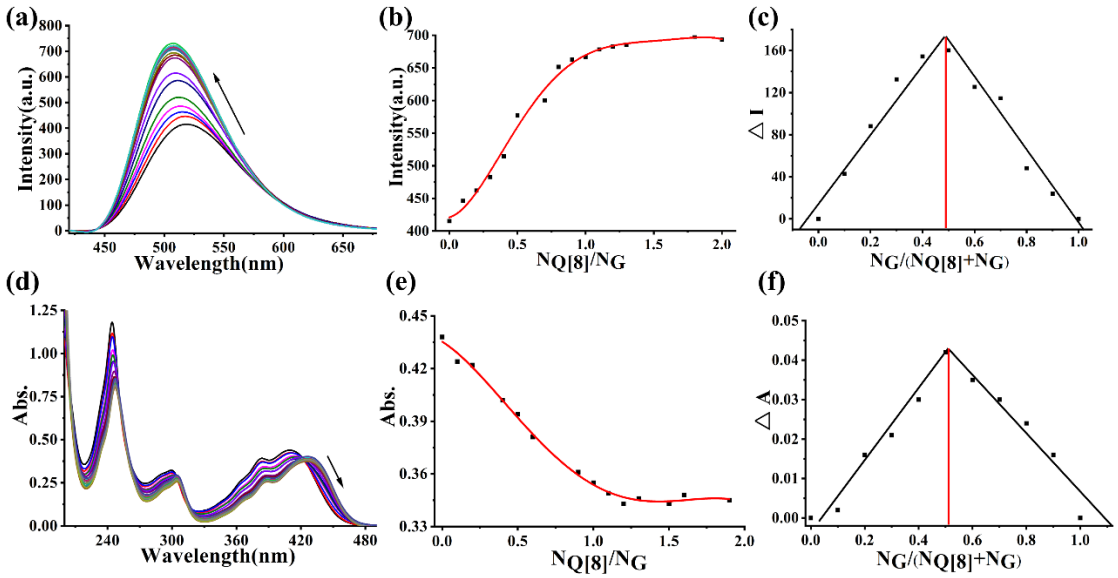

Figure 3. (a) Fluorescence spectra of G with increasing molar equivalents of Q[8] from 0, 0.1, 0.2, 0.3, 0.4, 0.5…to 2.0 (λ_{ex}=410 nm); (b) The corresponding I. *vs* $N_{Q[8]}/N_G$ curves ; (c) Job's plot for Q[8] with G; (d) UV-Vis spectroscopy of G with increasing molar equivalents of Q[8] from 0, 0.1, 0.2, 0.3, 0.4, 0.5…to 2.0; (e) The corresponding A. *vs* $N_{Q[8]}/N_G$ curves; (f) Job's plot for Q[8] with G.

2.3. Detection and Removal for nitrophenol isomers

Due to G@Q[8] possessing favorable photophysical properties, it provides good conditions to construct a probe for detecting analytes. Hence, we tried to use it to detect nitrophenol isomers and the results showed that the probe can identify effectively *o*-NP from other nitrophenol isomers. As demonstrated in Figure S6, upon addition of *o*-NP to the solution of G@Q[8], the fluorescence spectra showed distinct changes in intensity and was accompanied by a minor bathochromic shift from 508 nm to 516 nm, while the other nitrophenol isomers were not significantly quenched the fluorescence. It can observed in Figure 4a, the quenching efficiency (QE) of the G@Q[8] toward these nitrophenol isomers is in the order *o*-NP > *p*-NP > *m*-NP. Obviously, *o*-NP as the analyte with the highest QE of up to 83.3% is distinctly larger than the other two and the QE of *o*-NP is about 2.4 times larger than that of its isomer *p*-NP (QE = 35.1%) and 6.2 times larger than that of *m*-NP (QE = 13.5%). Considering that high selectivity is an important index of a probe, the fluorescent quenching of the G@Q[8] to *o*-NP was studied in the presence of other nitrophenol isomers at the same concentration. When the *p*-NP or/and *m*-NP were mixed together with the

probe, this only induces a slight decrease of the fluorescence intensity. However, once *o*-NP was added to the complicated solution, the fluorescence of the probe was significantly quenched. All these results confirm that G@Q[8] can be employed as a distinguishable fluorescent probe for recognizing *o*-NP from its two isomers with high selectivity.

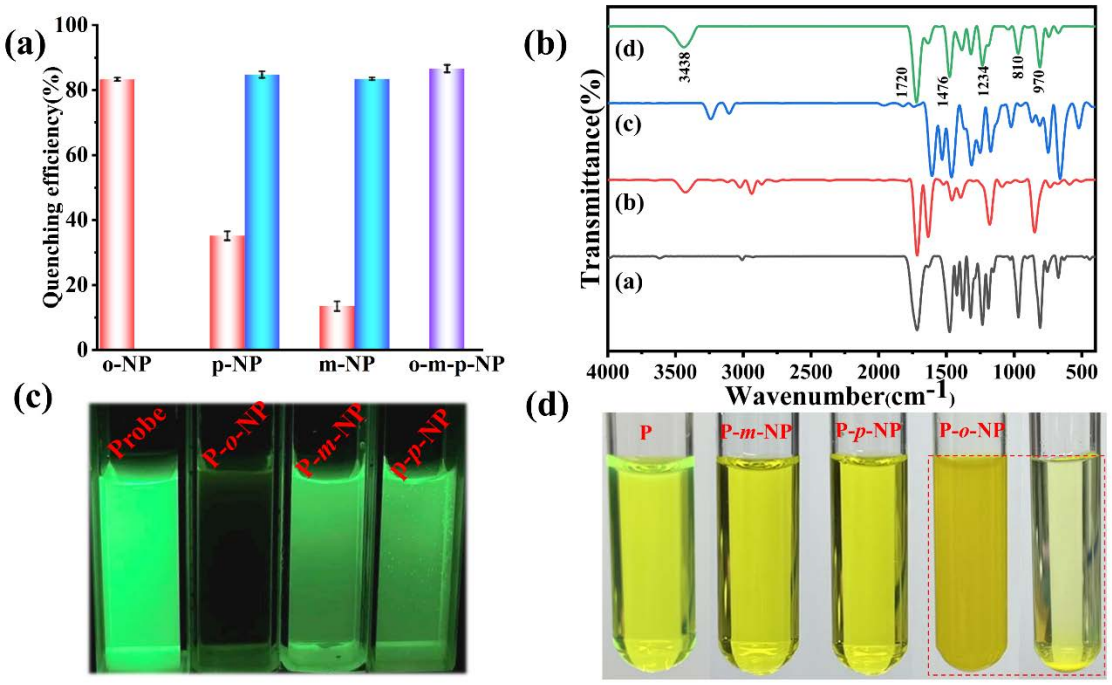

Figure 4. (a) Histogram of the fluorescence efficiency of probe G@Q[8] in the presence and absence of interferents. (red column: presence of only 15 equiv. *o*-NP, *m*-NP or *p*-NP; blue column: presence of both *o*-NP and *p*-NP or *m*-NP; Purple column: presence of all); (b) FT-IR spectra of (a-d) Q[8], G, *o*-NP and Precipitate; (c) Photographs of G@Q8 in the presence or absence of *o*-NP, *m*-NP and *p*-NP (15 equiv.) under UV light at 365 nm; (d) Photographs of G@Q8 and G@Q8 on addition of *m*-NP, *p*-NP and *o*-NP from left to right, respectively.

The quenching ability of G@Q[8] for *o*-NP was further investigated by incrementally addition of different concentrations. Figure 5a depicts the fluorescence emission spectra of G@Q[8] at different concentrations of *o*-NP in an aqueous medium, and it can be seen that the fluorescence emission intensity gradually decreases as the concentration of *o*-NP increases. The fluorescence intensity exhibited a good linear relationship with concentration of *o*-NP within a certain concentration range. It was calculated from Figure 5c that the detection limit (DL) of *o*-NP is 1.53×10^{-7}mol L^{-1}. The calculation method is given in Table S2. Most interestingly, the aqueous solution of G@Q[8] started to become cloudy and eventually formed a considerable amount of

precipitate with increasing concentration of *o*-NP, suggesting that the probe can not only recognize but can also remove it from the water, which was confirmed by the increasing size distributions in the dynamic light scattering (DLS) data (Figure S7). In order to observe this phenomenon more carefully, we added 15 equiv. *o*-NP, *m*-NP and *p*-NP to the probe (0.1mM), respectively, and it was found that the solution quickly became turbid after adding *o*-NP, which finally precipitated at the bottom of the test tube (Figure 4d). The precipitate was washed with 3M hydrochloric acid solution and distilled water, dried, and measured by Fourier Transform infrared spectroscopy. As shown in Figure 4b, the characteristic bands of G, Q[8] and *o*-NP can be observed in the IR spectrum of the precipitated product. The O-H stretching vibration appearing at 3438 cm^{-1}, which can be attributed to the carboxyl moiety of G. The band at 1720 cm^{-1} arises from the C=O stretching vibration of G and Q[8]. The bending vibration of methylene of Q[8] appears at 1476 cm^{-1}, the C−C stretching vibration and the deformation vibrations of the glycoluril ring appears at 970 cm^{-1} and 810 cm^{-1}, respectively. A wider band appeared at 1234 cm^{-1} belonging to the C-O stretching vibration of *o*-NP. Therefore, it can be said that the precipitate is a ternary complex.

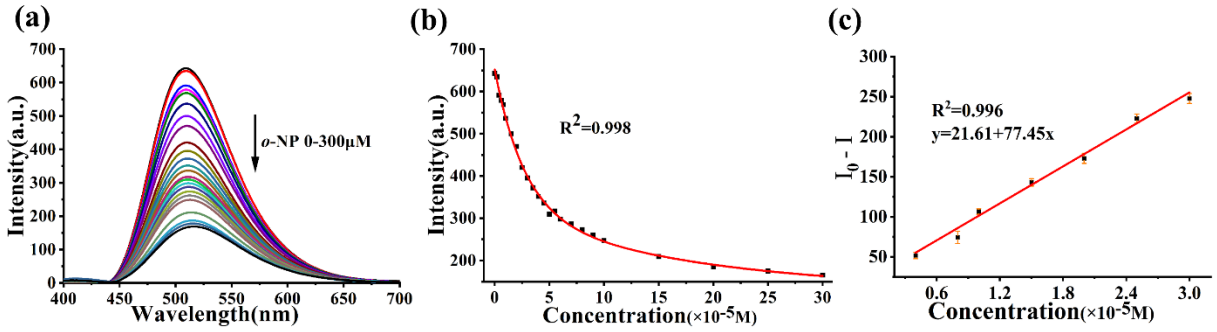

Figure 5. (a) Fluorescence emission spectra of G@Q[8] in the presence of different concentrations of *o*-NP in an aqueous medium (0-300μM); (b) the corresponding I *vs.* C curves; (c) Plot of DL.

2.4. Method validation in real sample

Subsequent feasibility analysis of the established analytical method using river water of Huaxi (Guiyang, Guizhou, China) as a real sample, including linearity, precision (inter- and intra-day), detection limit (DL) and recovery. After simple pretreatment, highspeed centrifugation to remove a small amount of sediment and 0.22μm filter filtration, the same analysis protocol was conducted to detect the *o*-NP in a 10μM probe solution. The method precision, including the intra- and inter-day precision, was determined upon repeated probe solution containing 20μM of *o*-NP.

The probe solution was analyzed five consecutive times to determine the intra-day precision and three consecutive days for the inter-day precision to evaluate the repeatability of the method. The calibration curve was plotted in terms of the fluorescence intensity *vs* concentration (Figure S8). Table 1 shows the intra-day precision was 0.13%, while the inter-day precision was 3.16%, the correlation coefficient, DL and linear range are 0.998, 4.24×10^{-7} M and 2.0-50.0μM, respectively, implying that *o*-NP also exhibited good linearity, precision and high sensitivity in river water. The recovery was used to estimate the accuracy of the method. The *o*-NP was not detected in non-spiked river water samples, therefore, the accuracy of the proposed analytical method was investigated by spiked river water sample at three different levels, and recoveries were calculated by comparing the final obtained concentration with the initial spiked concentration. Each recovery experiment was repeated three times and expressed as an average. As the results show in Table 2, recoveries for *o*-NP ranged from 105.1% to 107.2% with RSD<0.27%, demonstrating robust accuracy and reproducibility of the method. Further, the performance of G@Q[8] was compared with previously reported sensors (Table S3). It can be seen that the analysis method can realize the detection of the whole water system, the analysis parameters such as linear range and detection limit are good, and the detection method is simple and fast.

Table 1. Linear range, detection limit and precisions data for the determination of river water.

sample	RSD (%, n=5)	RSD (%, n=3)	Linear range	Correlation coefficient (R^2)	DL($*10^{-7}$M)
	Intra-day	Inter-day	2.0-50.0μM	0.998	4.24
river water	0.13	3.16			

Table 2. Recoveries of river water samples.

sample	Spiked (μM)	Found (μM)	RSD (%, n=3)	Recovery (%)
river water	6.0	6.4	0.27	107.2
	15.0	15.8	0.15	105.5
	25.0	26.3	0.05	105.1

2.5. Mechanism of fluorescence quenching.

The impressive detection and removal performance of G@Q[8] toward *o*-NP enabled us to further study the mechanism behind these processes. Firstly, we explored the interaction between the guest molecule G and *o*-NP, and the results showed there was no obvious change in fluorescence intensity when *o*-NP was added to an aqueous solution of G (Figure S10), which indicating that it is G@Q8 that can detect the *o*-NP rather than a single guest G. This conclusion was further verified by ^{1}H NMR spectroscopic titrations. As shown in Figure S11, after adding *o*-NP to the guest G at a concentration of 0.5 mM, the proton signals of G have no obvious chemical shift. By comparison, when adding *o*-NP into G@Q8 in an aqueous solution, the chemical shift of the proton signals of the pyrene moiety of G change significantly (Figure 6 and S12), with the signals of protons H_a, H_b and H_d showing a down-field shift, moving from δ= 8.84 ppm to δ= 8.92 ppm, δ= 8.28 ppm to δ =8.32 ppm and δ =7.36 ppm to δ= 7.46 ppm respectively. $H_{g\text{-}j}$ of the alkyl chain all revealed a down-field shift. Interestingly, H_e splits into two peaks and one peak moves up-field, the other moves down-field, while there is no significant change in the chemical shift of H_c. However, compared with free guest G, H_c, H_d, H_e all show an up-field shift, which indicates that the pyrene moiety of G is still located in cavity of the Q[8]. The proton signals of *o*-NP are not shown in the ^{1}H NMR spectra until it is added in excess, and compared with free *o*-NP, its proton signal peaks all exhibit up-field shifts, demonstrating that *o*-NP also enters the cavity of the Q[8] to form a ternary complex system. ^{1}H NMR titrations of Q[8]@G/*p*-NP and Q[8]@G/*m*-NP were conducted in the same way (Figure S13 and S14). By comparing the NMR titration spectra of G@Q[8] with *o*-NP, *m*-NP and *p*-NP, we find that the proton signal changes of guest G were consistent no matter which nitrophenol was added. However, the difference is that the addition of *o*-NP will significantly reduce the proton signal peaks of G@Q[8]. Then we tested the NMR titration of Q[8]/*o*-NP and found that with the continuous addition of Q[8], the peaks of *o*-NP began to decrease and then disappeared, which indicates that the formation of a ternary complex precipitate was mainly due to the interaction of Q[8] and *o*-NP (Figure S15). Based on the above experimental phenomena, we speculate that since the electropositive guest G possesses an inherent affinity toward the electron negative *o*-NP, when the pyrene moiety of G and the *o*-NP are in the cavity of Q[8] at the same time, a charge transfer interaction occurs between the pyrene ring and the nitro group of *o*-NP resulting in a stable ternary complex, and the cavity of Q[8] simultaneously promotes the π-π interaction between G and *o*-NP, which accelerates the electron transfer throughout the process and leads to effective fluorescence quenching[49-51]. Moreover, the

interaction between Q[8] and *o*-NP makes the formed ternary complex precipitate out of solution, further promoting the efficient fluorescence quenching of the probe.

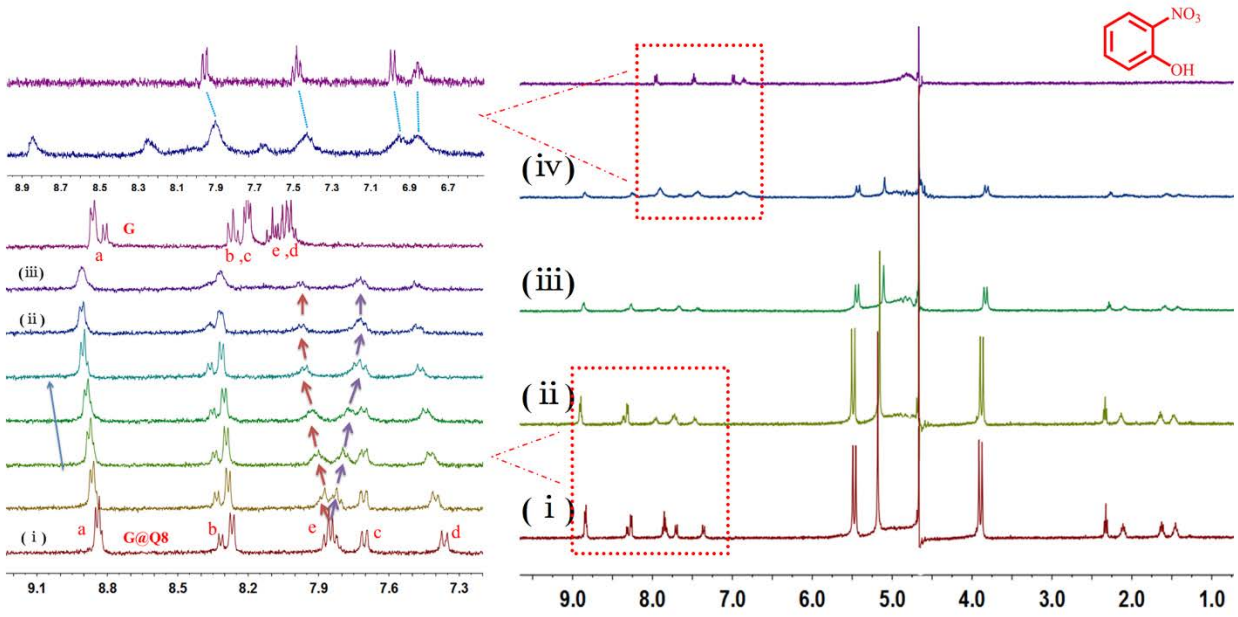

Figure 6. ^{1}H NMR spectra of G@Q[8] with *o*-NP: (i-iv) G@Q[8] with 0, 50, 200 μL, 400 μL *o*-NP (0.01M).

3. Conclusion

In summary, a water-soluble pyrene-based derivative with good fluorescence emission was designed and synthesized, and was used to construct a fluorescent probe G@Q[8] with a molar ratio of 1:1, which can selectively recognize and remove quickly *o*-NP among the nitrophenol isomers in aqueous solution; the detection limit is 1.53×10^{-7}mol/L. In addition, the formation of a ternary complex enables *o*-NP to precipitate rapidly from aqueous solution to achieve its removal. The possible mechanism of action was investigated and findings indicated that guest G and the electron-deficient *o*-NP can enters the cavity of Q[8] through charge transfer interaction. At the same time, the cavity promotes π-π interaction between G and *o*-NP, which effectively accelerates the electron transfer during the whole process and causes fluorescence quenching. Moreover, the interaction of Q[8] and *o*-NP promotes the formation of ternary complex precipitate, which further leads to efficient fluorescence quenching. This cucurbit[8]uril-based fluorescent probe provides a

fast and convenient method for the detection and removal of *o*-NP, and provides new insight into the application of host-guest assemblies for solving environmental pollution problems.

4. Experimental Section

General Comments: Q[8] was prepared and purified in our laboratory according to the literature procedure [45]. All other reagents and chemicals were purchased from common suppliers, and were of analytical grade and were used as received without further purification.

Measurements*:* The NMR spectra were recorded on a JEOL JNM-ECZ400s spectrometer using tetramethylsilane (TMS) as an internal reference with D_2O as the field-frequency lock and the chemical shifts are reported in parts per million (ppm). The fluorescence spectra of the host-guest complexes were recorded at 293.15K using a Varian Cary Eclipse spectrofluorometer, and UV-visible absorption spectra were recorded from samples in 1 cm quartz cells on an Agilent 8453 spectrophotometer at room temperature. Stock solutions of Q[8] (1.0×10^{-4} mol/L), G (1.0×10^{-3} mol/L) and nitrophenol isomers (1.0×10^{-3} mol/L) were prepared in double-distilled water. The test samples were prepared by diluting the stock solution, the solution of fixed G was 2.0×10^{-5} mol/L, and a certain proportion of Q[8] and nitrophenol isomer solution were added to prepare the final working sample. Single crystal data for compound G was collected on the Bruker D8 VENTURE diffractometer with graphite monochromatic Mo-Kα radiation (λ = 0.71073 Å). CCDC 2160405

Preparation of 6-bis(N-hexanoic acid pyridinium-4-yl) pyrene (G): To a solid mixture of 1,6-bis(4′-pyridyl)pyrene (1) (50.0 mg, 0.14 mmol) and 6-bromohexanoic acid (137.0 mg, 0.70 mmol) was added 15.0 ml acetonitrile and 5.0 ml toluene. The reaction mixture was refluxed for 12 h at 110 °C. The reaction mixture was then cooled to room temperature and the precipitate was then filtered, washed with diethyl ether and dried to give a green solid compound G (58.5 mg, 56%). 1H NMR (400 MHz, D_2O) δ(ppm): 8.79 (m, J = 24.0, 6.5 Hz, 4H), 8.07 (m, 6H), 7.84 (m, J = 11.2 Hz, 6H), 4.56 (t, 2H), 2.28 (t, J = 7.2 Hz, 4H), 2.00 (m, 4H), 1.63-1.52 (m, 4H), 1.33 (m, 4H).

Measurement of the limit of detection: The calculation method used for the detection limit (DL) was based on the standard derivation of 11 measurements in the absence of the guest molecule (σ) and the slope of the linear calibration curve (K) according to the formula: DL=3σ/K

AUTHOR INFORMATION

Corresponding Author

Xin Xiao-Key Laboratory of Macrocyclic and Supramolecular Chemistry of Guizhou Province, Guizhou University, Guiyang 550025, China.

Email: gyhxxiaoxin@163.com

Author Contributions

Jiao He: Validation and writing - original draft; Xiang-Yun Yu: Resources; Zhi-Chao Yu: crystal structure data analysis; Ming Liu: Investigation; Pei-Hui Shan: Resources; Carl Redshaw: Writing - review & editing; Ying Huang: Supervision; Zhu Tao: Supervision; Xin Xiao: Conceptualization.

Notes

The authors declare no competing financial interest.

ACKNOWLEDGMENT

This work was supported by the National Natural Science Foundation of China (No. 21861011, 22061009) and the Innovation Program for High-level Talents of Guizhou Province (No. 2016-5657). CR thanks the EPSRC for an Overseas Travel Grant (EP/R023816/1).

REFERENCES

[1] Z.X. Zhang, J. Zhou, Y. Liu, J. Tang, W.H. Tang, Cyclodextrin capped CdTe quantum dots as versatile fluorescence sensors for nitrophenol isomers. *Nanoscale* 2015, 7, 19540.

[2] M. Murphy, D. Manoj, D. Saravanakumar, K. Thenmozhi, S. Senthilkumar, Water insoluble, self-binding viologen functionalized ionic liquid for simultaneous electrochemical detection of nitrophenol isomers. *Anal. Chim. Acta* 2020, 1138, 89.

[3] Y. Huang, S. Bai, J. Huang, Y. Ma, Q. Zeng, M. Wang, L. Wang, Simultaneous detection of nitrophenol isomers using an easy-to-fabricate thiophene based microporous polymer film modified electrode. *Microchemical Journal* 2020, 153, 104465.

[4] B. Thirumalraj, C. Rajkumar, S. M. Chen, K. Y. Lin, Determination of 4-nitrophenol in water by use of a screen-printed carbon electrode modified with chitosan-crafted ZnO nanoneedles. *Journal of Colloid and Interface Science* 2017, 499, 83.

[5] J. Zhan, H. Wang, X. Pan, J. Wang, Y. Wang, Simultaneous regeneration of p-nitrophenol-saturated activated carbon fiber and mineralization of desorbed pollutants by electro-peroxone process. *Carbon* 2016, 101, 399.

[6] Y. Ji, Y. Shi, Y. Yang, P. Yang, L. Wang, J. Lu, L. Zhou, C. Ferronato, J. M. Chovelon, Rethinking sulfate radical-based oxidation of nitrophenols: formation of toxic polynitrophenols, nitrated biphenyls, and diphenyl ethers. *J. Hazard. Mater* 2019, 361, 152.

[7] W. Yue, M. Chen, Z. Cheng, L. Xie, M. Li, Bioaugmentation of strain methylobacterium sp. C1 towards p-nitrophenol removal with broad spectrum coaggregating bacteria in sequencing batch biofilm reactors. *J. Hazard. Mater* 2018, 344, 431.

[8] W. Shen, Y. Qu, X. Pei, S. Li, S. You, J. Wang, Z. Zhang, J. Zhou, Catalytic reduction of 4-nitrophenol using gold nanoparticles biosynthesized by cell-free extracts of aspergillus sp. WL-Au. *J. Hazard. Mater* 2017, 321, 299.

[9] Y. Wang, Q. Li, P. Zhang, D. O'Connor, R.S. Varma, M. Yu, One-pot green synthesis of bimetallic hollow palladium-platinum nanotubes for enhanced catalytic reduction of p-nitrophenol. *J. Colloid Interface Sci* 2019, 539, 161.

[10] L. Han, S. G. Liu, J. Y. Liang, Y. J. Ju, N. B. Li, H.Q. Luo, pH-mediated reversible fluorescence nanoswitch based on inner filter effect induced fluorescence quenching for selective and visual detection of 4-nitrophenol. *J. Hazard. Mater* 2019, 362, 45.

[11] C. Yin, J. Cai, L. Gao, J. Yin, J. Zhou, Highly efficient degradation of 4-nitrophenol over the catalyst of Mn_2O_3/AC by microwave catalytic oxidation degradation method. *J. Hazard. Mater* 2016, 305, 15.

[12] X. Ma, Y. Wu, S. Devaramani, C. Zhang, X. Lu, Preparation of GO-COOH/AuNPs/ZnAPTPP nanocomposites based on the π-π conjugation: Efficient interface for low-potential photoelectrochemical sensing of 4-nitrophenol. *Talanta* 2018, 178, 962.

[13] T. Wei, X. Huang, Q. Zeng, L. Wang, Simultaneous electrochemical determination of nitrophenol isomers with the polyfurfural film modified glassy carbon electrode. *J. Electroanal. Chem* 2015, 743, 105.

[14] C. Borr´as, T. Laredo, J. Mostany, B. R. Scharifker, Study of the oxidation of solutions of p-chlorophenol and p-nitrophenol on Bi-doped PbO_2 electrodes by UV-Vis and FTIR in situ spectroscopy. *Electrochim. Acta* 2004, 49, 641.

[15] Z. Y. Gu, X. P. Yan, Metal-organic framework MIL-101 for high-resolution gas chromatographic separation of xylene isomers and ethylbenzene. *Angew. Chem. Int. Ed* 2010, 48, 1477.

[16] S. M. Xie, N. Fu, L. Li, B. Y. Yuan, J. H. Zhang, Y. X. Li, L. M. Yuan, Homochiral metal-organic cage for gas chromatographic separations. *Anal. Chem*. 2018, 90, 9182.

[17] J. J. Wei, Y. J. Guo, J. Z. Li, M. K. Yuan, T. F. Long, Z. D. Liu, Optically active ultrafine Au-Ag alloy nanoparticles used for colorimetric chiral recognition and circular dichroism sensing of enantiomers. *Anal. Chem* 2017, 89, 9781.

[18] Y. W. Zhao, Y. Wang, X. M. Zhang, Homochiral MOF as circular dichroism sensor for enantioselective recognition on nature and chirality of unmodified amino acids. *ACS Appl. Mater. Interfaces* 2017, 9, 20991.

[19] R. J. He, J. Fan, Q. Tan, Y. C. Lai, X. D. Chen, T. Wang, Y. Jiang, Y. M. Zhang, W. G. Zhang, Enantioselective determination of metconazole in multi matrices by high-performance liquid chromatography. *Talanta* 2018, 178, 980.

[20] X. P. Tan, G. F. Zhao, X. Zhou, T. H. Li, H. Lei, G. B. Du, L. Yang, Electrochemical recognition of nitrophenol isomers by assembly of pillar[5]arenes mutifilms. *Anal. Chim. Acta* 2018, 1036, 49.

[21] M. Y. Yu, J. H. Liu, C. Liu, W. Y. Pei, J. F. Ma, Resorcin[4]arene-based microporous metal-organic framework/reduced graphene oxide composite as an electrocatalyst for effective and simultaneous determination of p-nitrophenol and o-nitrophenol isomer. *Sensor Actuat B: Chem* 2021, 347, 130604.

[22] Y. Wu, W. P. Zhang, Z. L. Chen, A poly (4-vinylpridine-co-ethylene glycol dimethacrylate) monolithic concentrator for in-line concentration-capillary electrophoresis analysis of phenols in water samples. *Electrophoresis* 2012, 3, 2911.

[23] H. Nie, Z. Wei, X. L. Ni, Y Liu. Assembly and Applications of Macrocyclic-Confinement-Derived Supramolecular Organic Luminescent Emissions from Cucurbiturils. *Chem. Rev* 2022, 122, 9032.

[24] W. Wu, S. Song, X. W. Cui, T. Sun. J. X. Zhang, X. L. Ni. pH-Switched fluorescent pseudorotaxane assembly of cucurbit[7]uril with bispyridinium ethylene derivatives. *Chinese Chem. Lett*, 2018, 29, 95.

[25] P. Wang, S. X. Cao, T. Yin, X. L. Ni. Unprecedented tunable hydrophobic effect and anion recognition triggered by AIE with Hofmeister series in water. *Chinese Chem. Lett*, 2021, 32, 1679.

[26] T. Yin, S. Zhang, M. X. Li, C. Redshaw, X. L. Ni, Macrocycle encapsulation triggered supramolecular pKa shift: A fluorescence indicator for detecting octreotide in aqueous solution. *Sensor Actuat B: Chem* 2019, 281: 568.

[27] X. M. Du, B. Zhao, Q. Yang, J. S. Wang, F. Y. Xie, H. Y. Yu, Y. Li, Y. X. Ma, W. J. Ruan, Dual-emissive dye@MOF composite for ratiometric detection and discrimination of two isomers of tetrachlorobenzenediol. *New J. Chem* 2020, 44, 20871.

[28] H. Yang, F. Lu, Y. Sun, Z. Yuan, C. Lu, Fluorescent gold nanocluster-based sensor array for nitrophenol isomer discrimination via an integration of host-guest interaction and inner filter effect. *Anal. Chem* 2018, 90, 12846.

[29] J. Zhang, J. Wang, S. Long, S. B. Peh, J. Dong, Y. Wang, A. Karmakar, Y. D. Yuan, Y. Cheng, D. Zhao, Luminescent metal-organic frameworks for the detection and discrimination of o-xylene from xylene isomers. *Inorg. Chem* 2018, 57, 13631.

[30] Z. Lu, X. Lu, Y. Zhong, Y. Hu, G. Li, R. Zhang, Carbon dot-decorated porous organic cage as fluorescent sensor for rapid discrimination of nitrophenol isomers and chiral alcohols. *Anal.Chim. Acta* 2019, 1050, 146.

[31] M. Liu, J. L. Kan, Y. Q. Yao, Y. Q. Zhang, B. Bian, Z. Tao, Q. J. Zhu, X. Xiao Facile preparation and application of luminescent cucurbit[10]uril-based porous supramolecular frameworks. *Sensor Actuat B: Chem* 2019, 283, 290.

[32] M. Liu, L. X. Chen, P. H. Shan, C. J. Lian, Z. H. Zhang, Y. Q. Zhang, Z. Tao, X. Xiao, Pyridine Detection Using Supramolecular Organic Frameworks Incorporating Cucurbit[10]uril. *ACS Appl. Mater. Inter* 2021, 13, 7434.

[33] D. Yang, M. Liu, X. Xiao, Z. Tao, C. Redshaw, Polymeric self-assembled cucurbit[n]urils: Synthesis, structures and applications. *Coordin. Chem. Rev* 2021, 434, 213733.

[34] Y. Luo, W. Zhang, M. Liu, J. Zhao, Y. Fan, B. Bian, Z. Tao, X. Xiao, A supramolecular fluorescent probe based on cucurbit[10]uril for sensing the pesticide dodine. *Chinese Chem. Lett* 2021, 32, 367.

[35] C. B. Achikanath, P. Haridas, M. Jyotirmayee, Cucurbit[n]uril based supramolecular assemblies: tunable physico-chemical properties and their prospects. *Chem. Commun* 2011, 47, 9959.

[36] Y. Yu, Y. Li, X. Wang, H. Nian, L. Wang, J. Li, Y. Zhao, X. Yang, S. Liu, L. Cao, Cucurbit[10]uril-Based[2]Rotaxane: Preparation and Supramolecular Assembly-Induced Fluorescence Enhancement. *J. Org. Chem* 2017, 82, 5590.

[37] D. Ma, G. Hettiarachchi, D. Nguyen, B. Zhang, J. B. Wittenberg, P. Y. Zavalij, V. Briken, L. Isaacs, Acyclic cucurbit[n]uril molecular containers enhance the solubility and bioactivity of poorly soluble pharmaceuticals. *Nat. Chem* 2012, 4, 503.

[38] C. Hu, N. Ma, F. Li, Y. Fang, Y. Liu, L. Zhao, S. Qiao, X. Li, X. Jiang, T. Li, F. Shen, Y. Huang, Q. Luo, J. Liu, Cucurbit[8]uril-Based Giant Supramolecular Vesicles: Highly Stable, Versatile Carriers for Photoresponsive and Targeted Drug Delivery. *ACS Appl. Mater. Interfaces* 2018, 10, 4603.

[39] Y. H. Liu, Y. M. Zhang, H. J. Yu, Y. Liu, Cucurbituril-Based Biomacromolecular Assemblies. *Angew. Chem. Int. Ed* 2021, 60, 3870.

[40] S. H. Li, X. Xu, Y. Zhou, Q. Zhao, Y. Liu, Reversibly Tunable White-Light Emissions of Styrylpyridiniums with Cucurbiturils in Aqueous Solution. *Org. Lett* 2017, 19, 6650.

[41] L. Ding, Y. Fang, Chemically assembled monolayers of fluorophores as chemical sensing materials. *Chem. Soc. Rev* 2010, 39, 4258.

[42] S. Wang, Y. Yang, X. Shi, L. Liu, W. Chang, J. Li, Multiple Stimuli-Responsiveness Fluorescent Probe Derived from Cyclopolymers and Pyrene-Ended Ammonium Salts. *ACS Appl. Polym. Mater* 2020, 2, 2246.

[43] S. Karuppannan, J. C. Chambron, Supramolecular chemical sensors based on pyrene monomer-excimer dual luminescence. *Chem. Asian J* 2011, 6, 964.

[44] E. Manandhar, K. J. Wallace, Host-guest chemistry of pyrene-based molecular receptors. *Inorg. Chim. Acta* 2012, 381, 15.

[45] S. J. Kim, I. S. Jung, S. Y. Kim, E. Lee, J. Kim, S. Sakamoto, K. Yamaguchi, K. Kim, Macrocycles within macrocycles: cyclen, cyclam, and their transition metal complexes encapsulated in cucurbit[8]uril. *J. Am. Chem. Soc* 2000, 122, 540.

[46] Q. Lu, G. K. Kole, A. Friedrich, K. M. Buschbaum, Z. Q. Liu, X. Q. Yu, T. B. Marder, Comparison Study of the Site-Effect on Regioisomeric Pyridyl-Pyrene Conjugates: Synthesis, Structures, and Photophysical Properties. *J. Org. Chem* 2020, 85, 4256.
[47] T. Jiang, X. Wang, J. Wang, G. P. Hu, X. Ma, Humidity and Temperature-Tunable Multicolor Luminescence of Cucurbit[8]uril-Based Supramolecular Assembly. *ACS Appl. Mater. Interfaces* 2019, 11, 14399.
[48] E. Freire, O. L. Mayorga, M. Straume, Isothermal titration calorimetry. *Anal Chem* 1990, 62, 950A.
[49] J. B. Chaires, Calorimetry and Thermodynamics in Drug Design. *Annu. Rev. Biophys* 2008, 37, 135.
[50] D. Zou, S. Andersson, R. Zhang, S. Sun, B. Åkermark, L. Sun, A Host-Induced Intramolecular Charge-Transfer Complex and Light-Driven Radical Cation Formation of a Molecular Triad with Cucurbit[8]uril. *J. Org. Chem* 2008, 73, 3775.
[51] L. Yang, H. Yang, F. Li, X. Zhang, Supramolecular glycolipid based on host-enhanced charge transfer interaction. *Langmuir* 2013, 29, 12375.